RESEARCH ARTICLE

Electronic, vibrational, and charge-transport properties of benzothienobenzothiophene–TCNQ co-crystals†‡

Ajith Ashokan, [iD] [a] Caitlin Hanson, [iD] §[a] Nathan Corbin, [iD] ¶[a] Jean-Luc Brédas [iD] ★[ab] and Veaceslav Coropceanu [iD] ★[ab]

The electronic, vibrational, and charge-transport properties of a series of benzothieno-benzothiophene (BTBT)–F_mTCNQ (m = 0, 2, 4) and diC$_n$BTBT–F_mTCNQ (n = 8, 12; m = 0, 4) donor–acceptor (DA) co-crystals have been investigated by means of density functional theory calculations. The electronic-structure calculations predict wide conduction bands and small effective masses for electrons along the DA stacking directions. The results indicate that the increase in the number of F atoms on the acceptor molecules results in an increase of superexchange couplings along the DA stacks, while the addition of the alkyl side chains results in a decrease of through-space transfer integrals between neighboring stacks. Time-dependent density functional theory calculations of the optical properties describe the lowest two optical transitions as having a charge-transfer character and being related to the two electronic coupling pathways that contribute to the superexchange couplings. The results also indicate that the ionicity parameter in the diC$_n$BTBT–F_mTCNQ cocrystals is somewhat larger than in the BTBT analogues. Overall, we find that DFT calculations based on periodic boundary conditions are a reliable tool to estimate the ionicity parameter in DA cocrystals.

1. Introduction

Over the last two decades, π-conjugated organic materials have attracted considerable attention for potential applications in various optoelectronic devices[1–5] with organic donor–acceptor (DA) co-crystals being considered as promising materials for OFET (organic field-effect transistor) applications.[6–20] In the case of binary molecular systems, the latter consist of a regular arrangement of D and A molecular moieties with a defined stoichiometry. Usually, DA co-crystals display a ground-state charge transfer (CT) configuration ($D^{\rho+}$–$A^{\rho-}$) with a partial ionicity.

The ionicity parameter (ρ) plays a critical role in defining the optical, electronic, and electrical properties of co-crystals, with ρ strongly correlated to the crystal packing motif. In binary crystals with 1 : 1 stoichiometry, two types of molecular stacking patterns are typically found: (i) segregated stacks, in which the D and A moieties align in separate, well-ordered stacks, –D–D–D– and –A–A–A–; and (ii) mixed stacks, in which the D and A moieties alternate along the stacking directions.[7] Segregated co-crystals are characterized by ρ values around 0.5 and predominantly exhibit metallic-like electrical properties; mixed-type co-crystals are usually semiconductors when $\rho < 0.5$ or insulators when $\rho \sim 1$.[6–9]

In recent years, benzothieno[3,2-*b*][1]benzothiophene (BTBT, see Fig. 1) and its alkylated derivatives have found wide applications as p-type semiconducting materials for OFET devices. In their pristine form, BTBT crystals show a high degree of layered crystallinity which facilitates hole transport and leads to mobilities up to 10 cm^2 V^{-1} s^{-1}.[21–23] Recently, it was found that BTBT and its derivatives can form DA cocrystals with 7,7,8,8-tetracyano-quinodimethane (TCNQ) and its fluorinated derivatives.[24–29] Interestingly, in contrast to the p-channel transport found in the BTBT crystals, the BTBT-based DA cocrystals mostly exhibit n-channel characteristics.[25–29]

A few theoretical studies have been reported on BTBT–TCNQ co-crystals.[24,25,29–31] However, the calculations of the

[a] *School of Chemistry and Biochemistry & Center for Organic Photonics and Electronics (COPE), Georgia Institute of Technology, Atlanta, Georgia 30332-0400, USA*

[b] *Department of Chemistry and Biochemistry, The University of Arizona, Tucson, Arizona 85721-0088, USA. E-mail: jlbredas@arizona.edu, coropceanu@arizona.edu*

† This article is dedicated to our mentor and friend Professor Fred Wudl, who has been at the forefront of design and synthesis of organic semiconducting and metallic materials for the past fifty years.

‡ Electronic supplementary information (ESI) available. See DOI: 10.1039/d0qm00420k

§ Department of Chemistry and Biochemistry, The University of Alabama, Tuscaloosa, Alabama 35487, USA.

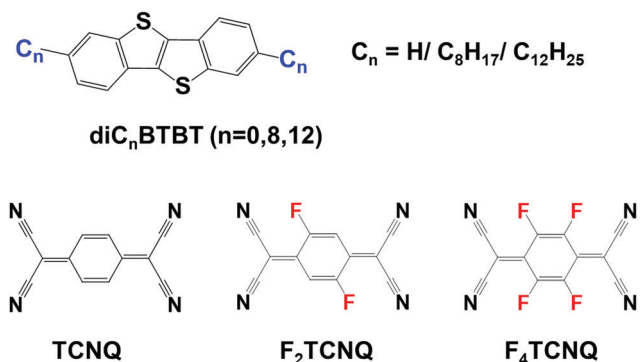¶ Department of Chemical Engineering, Massachusetts Institute of Technology, Cambridge, Massachusetts 02142, USA.

This journal is © The Royal Society of Chemistry and the Chinese Chemical Society 2020

Mater. Chem. Front., 2020, **4**, 3623–3631 | **3623**

Fig. 1 Chemical structures of the BTBT (n = 0, $C_n \equiv H$), diC$_8$BTBT ($C_8 \equiv C_8H_{17}$), and diC$_{12}$BTBT ($C_{12} \equiv C_{12}H_{25}$) donors as well as the TCNQ, F$_2$TCNQ, and F$_4$TCNQ acceptor molecules.

electronic-structure properties had so far been limited to the evaluation of the electronic couplings. Here, we greatly expand on these initial investigations and perform a detailed study of the electronic, optical, vibrational, and charge-transport properties of a series of BTBT–F$_m$TCNQ (m = 0, 2, 4) and diC$_n$BTBT–F$_m$TCNQ (n = 8, 12; m = 0, 4) co-crystals, see Fig. 1 (we note that the diC$_8$BTBT–F$_2$TCNQ and diC$_{12}$BTBT–F$_2$TCNQ crystals are not considered here due to the positional disorder of the F atoms in their experimental crystal structures).

2. Methodology

The geometry optimizations and calculations of the individual molecular energies of BTBT, diC$_n$BTBT (n = 8, 12), and F$_m$TCNQ (m = 0, 2, 4) were performed at the density functional theory (DFT) B3LYP/6-31G(d,p) level. Time-dependent density functional theory (TDDFT) was then used with the same functional and basis set to calculate the electronic excitations from the ground state. A natural transition orbital (NTO) analysis was applied to characterize the electronic excitations.[32] All these calculations were performed with the Gaussian 09-D01 package.[33]

The geometry optimizations of the DA co-crystals were also conducted at the DFT B3LYP/6-31G(d,p) level. In the course of the optimizations, the cell parameters were kept fixed at their experimental values while the atomic positions were allowed to relax. Harmonic vibrational frequencies were calculated at the Γ point of the co-crystals. The coupled perturbed Hartree–Fock/Kohn–Sham (CPHF/CPKS) approach[34] was used for the calculation of the vibrational spectra and the determination of the IR and Raman intensities. These calculations were carried out with the CRYSTAL 17 package.[35]

DFT B3LYP/6-31G(d,p) electronic band structures and densities of states (DOS) were calculated with the CRYSTAL 14 package.[36] In order to compare our results with previous studies, the electronic-structure calculations of the co-crystals were performed as well using the experimental crystal structures.[37] Uniform 8 × 8 × 8 or 8 × 8 × 4 Monkhorst–Pack k-point meshes were employed for the BTBT–F$_m$TCNQ (m = 0, 2, 4) and diC$_n$BTBT–F$_m$TCNQ (n = 8, 12 and m = 0, 4) co-crystals, respectively.

The electronic couplings between nearest-neighbor pairs of donor–donor, donor–acceptor, and acceptor–acceptor components were evaluated with a fragment orbital approach in combination with a basis set orthogonalization procedure.[38] The electronic couplings between D molecules [or A molecules] along the stacking directions were also estimated via an energy-splitting approach by considering the energy levels of a D–A–D [or A–D–A] triad:[8]

$$t^{\text{eff}} = \frac{E_{\text{H[L+1]}} - E_{\text{H−1[L]}}}{2} \tag{1}$$

where $E_{\text{H[L]}}$ and $E_{\text{H−1[L+1]}}$ are the energies of the HOMO[LUMO] and HOMO−1[LUMO+1] levels taken from the neutral state of the D–A–D [or A–D–A] triad. These calculations were carried out at the DFT B3LYP/6-31G(d,p) level using the Gaussian 09-D01 package.[33]

We recall that the inverse effective mass tensor of a crystal, m_{ji}^{-1}, is defined as:[39]

$$\frac{1}{m_{ij}} = \frac{1}{\hbar^2}\left(\frac{\text{d}^2 E}{\text{d}k_j \text{d}k_i}\right) \tag{2}$$

where subscripts i and j represent the Cartesian coordinates in reciprocal space; $\hbar$ is the reduced Planck constant and k, the electron wave-vector. The diagonalization of m_{ij}^{-1} provides the principal components and their orientations. The inverse effective mass tensor was calculated by means of Sperling's centered difference method with dk = 0.01 Bohr^{-1}.[8]

3. Results and discussion

3.1. Electronic structure

The crystal structures of BTBT–F$_m$TCNQ and diC$_n$BTBT–F$_m$TCNQ were taken from the Cambridge Structural Database (the unit-cell parameters are collected in Table S1 in the ESI‡).[25,28] BTBT–TCNQ, BTBT–F$_2$TCNQ, and diC$_n$BTBT–F$_m$TCNQ (n = 8, 12; m = 0, 4) co-crystals belong to the triclinic space group $P\bar{1}$, while the BTBT–F$_4$TCNQ co-crystal belongs to the monoclinic $P2_1/c$ space group. All co-crystals considered in this work are characterized by a 1 : 1 stoichiometry and crystallize as mixed stacks. The DA stacks in BTBT–TCNQ, BTBT–F$_2$TCNQ, and diC$_n$BTBT–F$_m$TCNQ co-crystals are located along the a crystallographic axis while those in BTBT–F$_4$TCNQ are along the b axis (see Fig. S1, ESI‡). In all systems, the donor and acceptor molecules are equidistant from each other along the stacking directions.

The electronic band structures and the densities of states of the co-crystals are given in Fig. 2 and 3, while Table 1 collects the widths of the conduction bands (CB) and valence bands (VB) along with the effective masses for each co-crystal (see also Table S2, ESI‡ for additional details). The CB widths are found to be significant, in the range of 280–380 meV, and are comparable to those already reported in the literature for co-crystals based on TCNQ and F$_4$TCNQ acceptors.[8,37] The largest values among the CB widths are estimated for the BTBT–F$_2$TCNQ, BTBT–F$_4$TCNQ, diC$_8$BTBT–F$_4$TCNQ, and di-C$_{12}$BTBT–F$_4$TCNQ co-crystals; this is due to the large
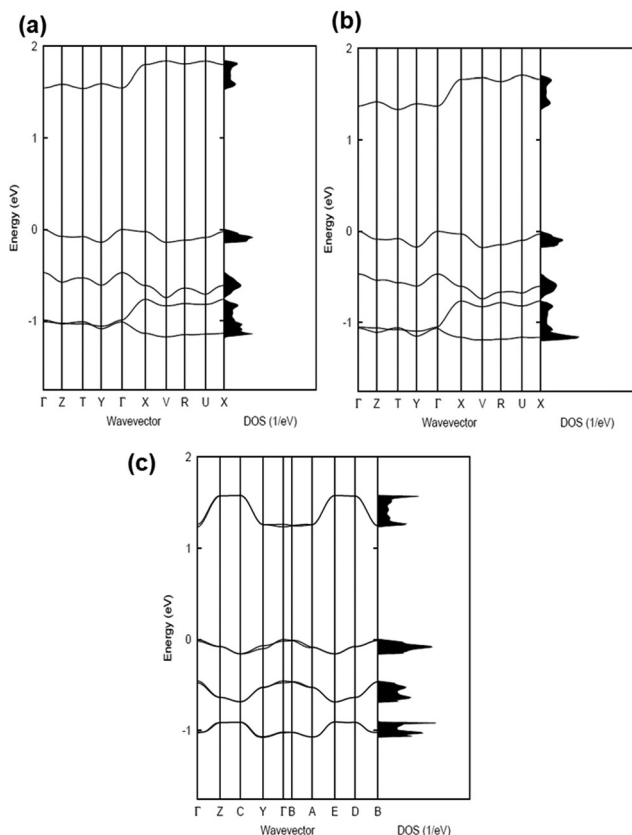
Fig. 2 Electronic band structures and densities of states (DOS) of the: (a) BTBT:TCNQ, (b) BTBT:F_2TCNQ, and (c) BTBT:F_4TCNQ co-crystals. The high-symmetry points in the first Brillouin zone are labelled as: Γ = (0, 0, 0), Z = (0, 0, 0.5), T = (0, 0.5, 0.5), Y = (0, 0.5, 0), X = (0.5, 0, 0), V = (0.5, 0.5, 0), R = (0.5, 0.5, 0.5), and U = (0.5, 0, 0.5) for the (a and b) cases and Γ = (0, 0, 0), Z = (0, 0.5, 0), C = (0.5, 0.5, 0), Y = (0.5, 0, 0), B = (0, 0, 0.5), A = (−0.5, 0, 0.5), E = (−0.5, 0.5, 0.5), and D = (0, 0.5, 0.5) for the (c) case. All points are given in fractional coordinates in reciprocal space. The zero of energy is taken as the top of the valence band.
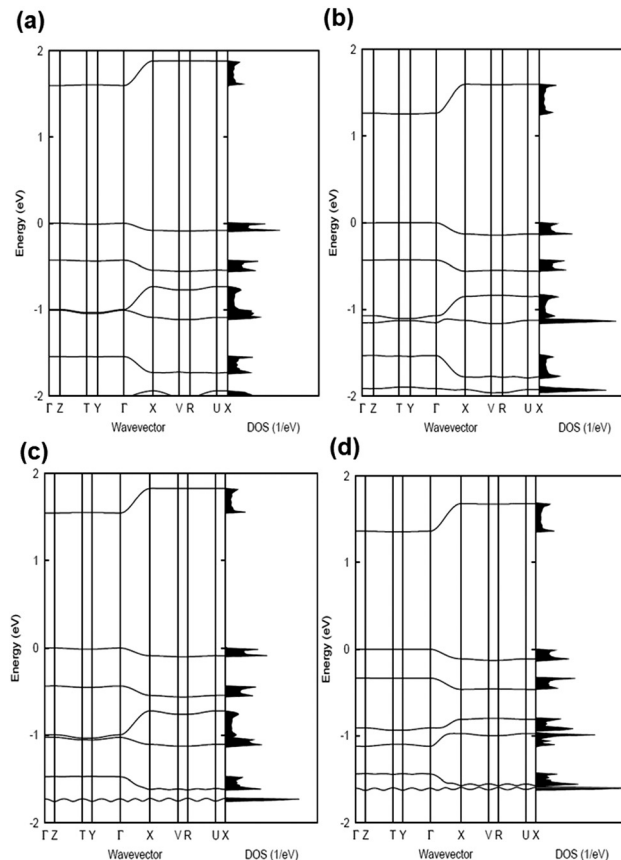

Fig. 3 Electronic band structures and densities of states (DOS) of the: (a) diC$_8$BTBT−TCNQ, (b) diC$_8$BTBT−F_4TCNQ, (c) diC$_{12}$BTBT−TCNQ, and (d) diC$_{12}$BTBT−F_4TCNQ co-crystals. The high-symmetry points in the first Brillouin zone are labelled as: Γ = (0, 0, 0), Z = (0, 0, 0.5), T = (0, 0.5, 0.5), Y = (0, 0.5, 0), X = (0.5, 0, 0), V = (0.5, 0.5, 0), R = (0.5, 0.5, 0.5), and U = (0.5, 0, 0.5) for all the co-crystals. All points are given in fractional coordinates in reciprocal space. The zero of energy is taken as the top of the valence band.

effective (superexchange) transfer integral ($\sim$60–80 meV) present along the stacking directions (see Table 2).

The VB widths fall in the range of 80–180 meV. In all investigated systems, the width of the VB is narrower than that of the CB. The largest band dispersions for the VB in BTBT–F_mTCNQ co-crystals are observed along directions perpendicular to the DA stacks. In contrast, in the co-crystals based on the diC$_n$BTBT donors, the largest VB band dispersions are observed along the stacking directions. The calculations show that, in BTBT–TCNQ and BTBT–F_2TCNQ co-crystals, the direct through-space electronic couplings ($t_{\mathrm{D–D}}$) related to hole transfer between BTBT molecules residing on adjacent DA stacks are much larger than the superexchange couplings ($t_{\mathrm{h}}^{\mathrm{eff}}$) along the stacking directions. In BTBT–F_4TCNQ, the $t_{\mathrm{D–D}}$ and $t_{\mathrm{h}}^{\mathrm{eff}}$ couplings are comparable and contribute nearly equally to the VB width. Overall, the calculations show that in all co-crystals the superexchange couplings for the electrons ($t_{\mathrm{e}}^{\mathrm{eff}}$) are much larger than those ($t_{\mathrm{h}}^{\mathrm{eff}}$) for the holes. As seen from Table 2, the values of both $t_{\mathrm{e}}^{\mathrm{eff}}$ and $t_{\mathrm{h}}^{\mathrm{eff}}$ in the co-crystals systematically increase with the increase in the number of F atoms

Table 1 B3LYP/6-31G(d,p) estimates of the full bandwidths (in parentheses, the related bandwidths along the DA stacking directions) of the conduction and valence bands along with the lowest two components of the effective masses (in units of electron mass in vacuum, m_0)

| Co-crystals | Bandwidth (in meV) | | Effective mass | | | |
| | | | Electrons | | Holes | |
	CB	VB	m_1/m_0	m_2/m_0	m_1/m_0	m_2/m_0
BTBT–TCNQ	299 (250)	139 (23)	1.0	3.2	1.3	4.7
BTBT–F_2TCNQ	372 (288)	177 (28)	0.8	1.5	1.0	3.4
BTBT–F_4TCNQ	345 (340)	157 (77)	0.8	3.6	2.1	2.3
diC$_8$BTBT–TCNQ	286 (280)	89 (82)	1.0	>10	3.1	>10
diC$_8$BTBT–F_4TCNQ	340 (329)	132 (128)	0.7	>10	1.5	>10
diC$_{12}$BTBT–TCNQ	283 (280)	100 (88)	1.2	7.5	3.9	>10
diC$_{12}$BTBT–F_4TCNQ	324 (316)	128 (110)	1.1	6.0	3.6	>10

on the acceptor molecule. This is due to the decrease in the D–A distances along the stacking directions in the co-crystals where the F_mTCNQ molecules have a larger number of fluorine atoms, see the crystallographic data in Table S2 (ESI‡).[25] We note that the dependence of the D–A distances on the number of fluorine

Table 2 B3LYP/6-31G(d,p) estimates (in meV) of the through space (holes – t_{D-D}, electrons – t_{A-A}), and superexchange (holes – t_h^{eff} and electrons – t_e^{eff}) transfer integrals (electronic couplings)

Co-crystals	t_{A-A}	t_{D-D}	t_e^{eff}	t_h^{eff}
BTBT–TCNQ	1.9	14.2	56.3	3.6
BTBT–F$_2$TCNQ	7.2	17.6	63.2	5.3
BTBT–F$_4$TCNQ	2.7	13.9	66.5	16.5
diC$_8$BTBT–TCNQ	0.7	4.7	67.2	17.6
diC$_8$BTBT–F$_4$TCNQ	3.3	1.1	78.1	34.7
diC$_{12}$BTBT–TCNQ	0.6	5.3	66.2	18.7
diC$_{12}$BTBT–F$_4$TCNQ	2.7	1.9	74.5	29.5

atoms can be attributed to the variations in halogen bonding; a strong impact of halogen bonding on crystal packing has been reported in DA co-crystals based on substituted benzoquinone acceptors.[14] The crystallographic data[25,28,29] also show that upon addition of the alkyl side chains (C$_n$), there occurs an increase in the separation distance between DA stacks. As a result, in contrast to the BTBT–F$_m$TCNQ co-crystals, the direct through-space transfer integrals for both holes and electrons in diC$_n$BTBT–F$_m$TCNQ co-crystals are significantly smaller than the corresponding superexchange couplings (see Table 2).

The smallest effective masses for electrons in all co-crystals are found along the stacking directions, which is consistent with the band structure and electronic-coupling results. Very small effective-mass values of $0.8m_0$, $0.8m_0$, and $0.7m_0$ (where m_0 is the rest mass of electrons in vacuum) are calculated for electrons along the mixed-stack directions in BTBT–F$_2$TCNQ, BTBT–F$_4$TCNQ, and diC$_8$BTBT–F$_4$TCNQ, respectively. The effective mass values for electrons in the other co-crystals are in the range of 1.0–$1.2m_0$. The effective masses for holes are larger than for electrons; however, in the BTBT–TCNQ, BTBT–F$_2$TCNQ, and diC$_8$BTBT–F$_4$TCNQ cases, the hole effective masses are still relatively small, falling in the range of 1.0–$1.5m_0$. We note that the smallest component of the effective mass for holes in the BTBT–F$_m$TCNQ ($m = 0, 2, 4$) co-crystals is oriented perpendicular to the stacking direction (see Table 1 and Table S2, ESI‡) while they are oriented along the mixed-stack directions in the diC$_n$BTBT–F$_m$TCNQ ($n = 8, 12; m = 0, 4$) co-crystals. These results imply that in BTBT–F$_m$TCNQ hole transport along the DA stacks is less effective than along other directions, a feature similar to that we recently found for co-crystals based on the 1,3,4,5,7,8-hexafluoro-11,11,12,12-tetracyanonaphtho-2,6-quinodimethane acceptor.[11]

Experimentally, based on OFET device measurements, Sato et al.[28] have found n-channel charge transport along the mixed-stack direction in the BTBT–F$_m$TCNQ ($m = 0, 2, 4$) single crystals, with the largest mobility of about 0.2 cm^2 V^{-1} s^{-1} observed in the case of BTBT–F$_4$TCNQ. Tsutsumi et al.[25] have also found predominately n-channel charge transport in OFET devices based on diC$_8$BTBT–F$_m$TCNQ ($m = 0, 2, 4$) co-crystals, with the largest electron mobility 0.4 cm^2 V^{-1} s^{-1}, measured along the DA stacks in diC$_8$BTBT–F$_2$TCNQ.[25] Our electronic-structure calculations are consistent with the experimental findings as they predict anisotropic electron transport properties (along the DA stacks) for all investigated systems.

Our calculations suggest that in addition to electron transport along the DA stacks, hole transport could be operational in the BTBT–TCNQ and BTBT–F$_2$TCNQ co-crystals along directions perpendicular to the DA stacks, and in the diC$_8$BTBT–F$_4$TCNQ co-crystal along the DA stacks. However, in OFET devices, hole mobilities were observed only in the case of the diC$_8$BTBT–TCNQ co-crystal and were measured to be very small.[25] We note that OFET mobilities depend on many other factors (disorder, domain boundaries, etc.) that should be considered for a detailed comparison between experiment and theory. For instance, in contrast to single-crystal results, the measurements performed on thin-film based devices show that all diC$_8$BTBT–F$_m$TCNQ systems display similar electron mobilities. In addition, we recall that our theoretical evaluations are based only on electronic-structure results and the role of electron–phonon interactions on charge mobility remains to be investigated.

3.2. Electron–hole asymmetry

A characteristic feature of many DA co-crystals is the "mirror symmetry" between the VBs and CBs in their band structures.[8] However, in the co-crystals considered here, the mirror symmetry between VB and CB is absent. A rationalization of why the electron–hole symmetry is observed in some co-crystals but is absent in others can be obtained by treating superexchange coupling in the perturbation limit. The superexchange couplings for holes and electrons in this limit are given as:

$$t_h^{eff} = \sum_{a_D(b_A)} \frac{t_{a_{D_1} b_A} t_{b_A a_{D_2}}}{E_{a_D b_A}} \qquad (3)$$

$$t_e^{eff} = \sum_{b_A(a_D)} \frac{t_{b_{A_1} a_D} t_{a_D b_{A_2}}}{E_{a_D b_A}} \qquad (4)$$

Here, a_D and b_A represent the molecular orbitals of the donor and acceptor (with $D_1[A_1]$ and $D_2[A_2]$ corresponding to two donor[acceptor] molecules in the D_1–A–D_2 [A_1–D–A_2] triad); $E_{a_D b_A}$ and $t_{a_D b_A}$ are the energy gaps and transfer integrals involving these orbitals.

When only the transfer integral from the HOMO (H_D) of the donor to the LUMO (L_A) of the acceptor contributes to the superexchange couplings, we obtain the well-established expression:

$$t_e^{eff} = t_h^{eff} = \frac{t_{H_D L_A}^2}{E_{H_D L_A}} \qquad (5)$$

Thus, in this case, the effective couplings for holes and electrons are equal. Generally, this occurs when the highest occupied molecular orbital (HOMO) and lowest unoccupied molecular orbital (LUMO) levels are energetically well separated from the rest of the molecular orbital levels. However, as first noticed by Tsutsumi et al.[25] for diC$_8$BTBT–F$_m$TCNQ and later found in other related systems,[27–29] both the HOMO and HOMO−1 of the donor are strongly interacting with the LUMO of the acceptor. Since the HOMO and HOMO−1 levels of BTBT are separated by only 0.3 eV (see Fig. 4), these two electronic-coupling pathways (i.e., HOMO$_D$ ⇒ LUMO$_A$, $t_{(H)D-(L)A}$ and HOMO−1$_D$ ⇒ LUMO$_A$, $t_{(H-1)D-LA}$) contribute to the super-exchange
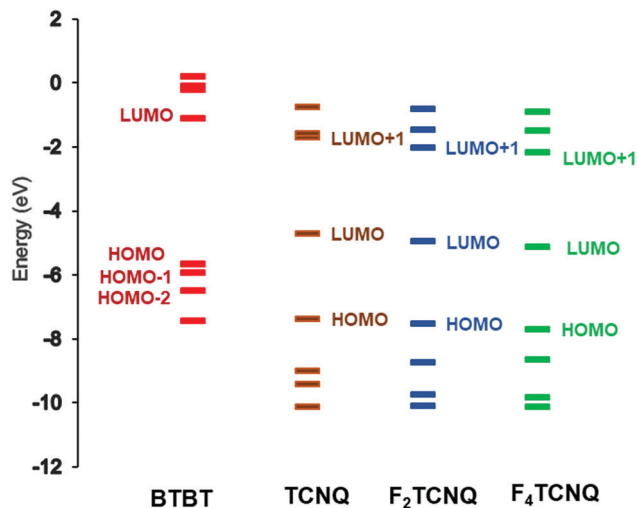
Fig. 4　Energy levels of the BTBT, TCNQ, F_2TCNQ, and F_4TCNQ molecules, as calculated at the B3LYP/6-31G(d,p) level.

couplings for electrons (t_e^{eff}). Indeed, the calculations by Zhu *et al.*[40] show that in the diC$_8$BTBT–F$_m$TCNQ systems the HOMO$_D$ ⇒ LUMO$_A$ and HOMO−1$_D$ ⇒ LUMO$_A$ interactions contribute nearly equally to the superexchange couplings for electrons (t_e^{eff}). Since the HOMO−1$_D$ ⇒ LUMO$_A$ coupling does not contribute to the superexchange couplings for holes, it is then expected that superexchange couplings should be larger for electrons than for holes ($t_e^{eff} > t_h^{eff}$); this results in electron–hole asymmetry in the electronic and charge-transport properties. The absence of a HOMO−1$_D$ ⇒ LUMO$_A$ contribution, however, does not fully explain why superexchange couplings in the BTBT–F$_m$TCNQ co-crystals are so small. Indeed, the estimation based on the derived $t_{(H)D-(L)A}$ and $t_{(H-1)D-(L)A}$ couplings (see Table 3) and eqn (3) and (4) indicate that t_e^{eff} in BTBT–TCNQ and BTBT–F$_2$TCNQ should be at most 4 and 3 times larger than t_h^{eff}, respectively. In reality, as seen from Table 2, the ratios t_e^{eff}/t_h^{eff} in the BTBT–TCNQ and BTBT–F$_2$TCNQ systems amount to 16 and 12, respectively. This result points to the existence of other electronic-coupling pathways for holes that act in a destructive way with respect to the HOMO$_D$ ⇒ LUMO$_A$ coupling. Calculations performed for the representative case of the BTBT–TCNQ co-crystal (see ESI,‡ Table S3) show that HOMO$_D$ ⇒ LUMO+1$_A$, HOMO$_D$ ⇒ LUMO+2$_A$, HOMO$_D$ ⇒ HOMO$_A$, HOMO$_D$ ⇒ HOMO−1$_A$,

HOMO$_D$ ⇒ HOMO−2$_A$, and HOMO$_D$ ⇒ HOMO−3$_A$ channels also contributes significantly to t_h^{eff}. Since these contributions have an opposite sign to the HOMO$_D$ ⇒ LUMO$_A$ contribution, they largely cancel the latter.

3.3. Charge-transfer optical transitions

As a result of donor–acceptor interactions, the DA systems usually exhibit charge-transfer (CT) excited states that are located below the donor and acceptor local excitations. The characteristics of the optical CT bands are directly related to the electronic couplings t_{DA} between the D and A frontier orbitals (and thus to the degree of ground-state ionicity). According to the Mulliken–Hush model,[41–43] the transition dipole moment (d_{CT}) of a CT band that peaks at E_{CT} is proportional to the ratio t_{DA}/E_{CT}. The diC$_8$BTBT–F$_m$TCNQ co-crystals exhibit two low-energy optical transitions with dipole moments parallel to the DA stacking direction, which were assigned as CT transitions related to HOMO$_D$ ⇒ LUMO$_A$ and HOMO−1$_D$ ⇒ LUMO$_A$ coupling channels.[25] Our excited-state calculations fully support this assignment, as the NTO analyses show that the first two optical transitions have a nearly 100% CT character (see Fig. S2, ESI‡). Our calculations indicate that two separate CT transitions should be observed in all the co-crystals considered here (see Table 4). The difference of 0.5–0.6 eV observed experimentally between the two CT transitions in the diC$_8$BTBT–F$_m$TCNQ co-crystals[25] is well reproduced by our calculations. In line with the experimental findings[25] our results also show that the CT transitions (see Table 4) exhibit a systematic redshift with the increase in the number of F atoms on the acceptor; this can be attributed to a corresponding decrease in the acceptor LUMO energy with the number of fluorine atoms (see Fig. 4). Taken together, our excited-state calculations and the experimental optical data provide strong support for the existence of comparable HOMO$_D$ ⇒ LUMO$_A$ and HOMO−1$_D$ ⇒ LUMO$_A$ contributions to the superexchange coupling in diC$_n$BTBT–F$_m$TCNQ co-crystals.

3.4. Ground-state ionicity

It is also of interest to quantify the ground-state ionicity (degree of charge transfer), ρ, in the current set of co-crystals. Vibrational spectroscopy is a commonly used tool to characterize ρ. In the case of the BTBT–F$_m$TCNQ co-crystals, Sato *et al.*[28] and Castagnetti *et al.*[29] used the IR C≡N and C=C stretching modes of the acceptor respectively, to estimate ρ. Here, in order

Table 3　B3LYP/6-31G(d,p) estimates of $t_{(H)_D-(L)_A}$ and $t_{(H-1)_D-L_A}$ where (H)$_D$ denotes HOMO of the donor molecule and L$_A$, is the LUMO of the acceptor molecule

Co-crystals	$t_{H_D-L_A}$ (meV)	$t_{(H-1)_D-L_A}$ (meV)
BTBT–TCNQ	160.3	348.1
BTBT–F$_2$TCNQ	226.7	329.5
BTBT–F$_4$TCNQ	252.4	331.9
diC$_8$BTBT–TCNQ	271.3	298.3
diC$_8$BTBT–F$_4$TCNQ	334.8	267.1
diC$_{12}$BTBT–TCNQ	271.2	289.3
diC$_{12}$BTBT–F$_4$TCNQ	327.1	266.7

Table 4　Excited-state energies of the co-crystals (in eV) calculated at the TDDFT B3LYP/6-31G(d,p) level. The values in parentheses are the corresponding oscillator strengths (f)

Co-crystals	S$_1$ (f)	S$_2$ (f)
BTBT–TCNQ	1.19 (0.0061)	1.78 (0.0620)
BTBT–F$_2$TCNQ	1.10 (0.0106)	1.65 (0.0616)
BTBT–F$_4$TCNQ	1.06 (0.0107)	1.61 (0.0666)
diC$_8$BTBT–TCNQ	1.16 (0.0164)	1.63 (0.0570)
di-C$_8$BTBT–F$_4$TCNQ	1.01 (0.0198)	1.43 (0.0634)
diC$_{12}$BTBT–TCNQ	1.13 (0.0171)	1.59 (0.0555)
di-C$_{12}$BTBT–F$_4$TCNQ	1.05 (0.0143)	1.42 (0.0641)

to provide additional insight on the ground-state ionicity, we computed the IR spectra, Raman spectra, and Mulliken molecular charges of the investigated co-crystals. The IR and Raman spectra are displayed in Fig. S3 and S4 (ESI‡), respectively. We estimated the ground-state ionicity parameter from the vibrational properties on the basis of two widely used approaches in the literature. The first approach is based on the formula:[44]

$$\rho = \frac{2(v_n - v_{DA})}{v_n(1 - v_a^2/v_n^2)} \quad (6)$$

Here, v_n, v_a, and v_{DA} are the frequencies of the acceptor vibrational mode of interest in the neutral, radical-anion, and co-crystal states, respectively. The second approach is based on the assumption of a linear dependence of v_{DA} on ρ, according to which:[45]

$$\rho = \frac{v_n - v_{DA}}{v_n - v_a} \quad (7)$$

We illustrate the application of these two approaches by considering the BTBT–F$_2$TCNQ co-crystal as a representative example. According to our calculations, the two most intense IR peaks from the antisymmetric C═C stretching modes are located at 1524 cm^{-1} and 1567 cm^{-1} in neutral F$_2$TCNQ, 1444 cm^{-1} and 1502 cm^{-1} in the radical-anion state of F$_2$TCNQ, and 1520 cm^{-1} and 1560 cm^{-1} in the BTBT–F$_2$TCNQ co-crystal. By substituting the average frequency values of the two modes in either eqn (6) or eqn (7), we obtain the same ρ value of 0.08, which agrees very well with the value of 0.09 reported by Castagnetti et al.[29] on the basis of the experimental IR spectra. We note, however, that the Dushinsky matrix[46] calculations (see ESI,‡ Table S4) show that the normal modes of the neutral and radical-anion states are highly intermixed; the high-frequency 1567 cm^{-1} mode of the neutral F$_2$TCNQ is found to have a larger projection coefficient on the 1444 cm^{-1} mode of the radical-anion state than on its 1502 cm^{-1} mode. If we consider 1567 cm^{-1}, 1444 cm^{-1}, and 1560 cm^{-1} as the values for v_n, v_a, and v_{DA} respectively, the linear scaling approach yields $\rho = 0.05$. In the case of the C≡N vibrations in the IR spectra, the two IR active modes are observed at 2226 cm^{-1} and 2240 cm^{-1} in the co-crystal, at 2233 cm^{-1} and 2251 cm^{-1} in neutral F$_2$TCNQ, and at 2176 cm^{-1} and 2208 cm^{-1} in the radical-anion state of F$_2$TCNQ. The use of eqn (6) and (7) yields ρ values of 0.19 and 0.18, respectively, which are slightly larger than the value of 0.16 derived by Sato et al.[28] from the experimental C≡N IR data. The ρ value estimated from the C≡N modes is thus larger than that estimated from the C═C stretching modes, which is not unexpected since it was suggested earlier that the approach based on C≡N modes systematically overestimates ρ.[28] The ρ values derived from DFT and experimental IR data for BTBT–F$_2$TCNQ are collected in Table 5, along with those for BTBT–TCNQ and BTBT–F$_4$TCNQ. The results indicate that the three systems share a similar ionicity parameter.

The ρ values estimated on the basis of Mulliken charges are also given in Table 5. In line with the results derived from the frequency-shift approach, similar ρ values are obtained for the co-crystals based on unsubstituted BTBT. However, the

Table 5 Degrees of charge transfer in the co-crystals based on Mulliken charges (ρ), as well as those derived from C═C mode ($\rho_{C═C}$) and C≡N mode ($\rho_{C≡N}$) analyses

Co-crystal	ρ	$\rho_{C═C}$		$\rho_{C≡N}$	
BTBT–TCNQ	0.04	0.08^a	0.10^b	0.19^a	0.20^c
BTBT–F$_2$TCNQ	0.04	0.08^a	0.09^b	0.18^a	0.16^c
BTBT–F$_4$TCNQ	0.04	0.09^a	0.12^b	0.13^a	0.11^c
diC$_8$BTBT–TCNQ	0.07	—	—	—	—
diC$_8$BTBT–F$_4$TCNQ	0.07	—	—	—	—
diC$_{12}$BTBT–TCNQ	0.06	—	—	—	—
diC$_{12}$BTBT–F$_4$TCNQ	0.05	—	—	—	—

^{a} Current work based on eqn (7). ^{b} From ref. 28. ^{c} From ref. 29.

Mulliken charge approach yields values that are about 60% smaller than the ones estimated from the vibrational frequency shifts. The co-crystals where BTBT has alkyl-chain substitutions display overall higher ρ values. The largest ρ value is calculated for the diC$_8$BTBT–F$_4$TCNQ system, which also shows one of the largest transfer integrals and conduction bandwidths along the stacking direction as well as one of the smallest effective masses for electrons. Moreover, diC$_8$BTBT–F$_4$TCNQ shows the largest OFET mobility values among the co-crystals in single-crystal based devices.[25] Finally, we note that the underestimation of ρ in the present calculations could be related to the use of the B3LYP functional. While we have previously shown that in DA co-crystals the super-exchange electronic couplings, the band structures, and the effective masses are not strongly affected by the choice of the DFT functional,[47] this might not be the case for the estimations of the ionicity parameter. Therefore, the implementation of range-separated hybrid functionals that are known to provide a reliable description of CT excitations[48,49] is desirable in order to obtain a better characterization of the co-crystal electronic properties in the context of periodic-boundary condition calculations.

4. Conclusions

We have investigated the electronic structure, vibrational properties, and charge-transport properties of co-crystals based on BTBT and di-C$_n$BTBT (n = 8, 12) donors and F$_m$TCNQ (m = 0, 2, 4) acceptors. The DFT calculations predict large conduction bandwidths and small effective masses for electrons in all co-crystals, which points to efficient electron transport in these systems. Large values of the valence bandwidths and small effective masses for holes are also observed for the BTBT–F$_m$TCNQ (m = 0, 2, 4) co-crystals, which suggests ambipolar transport characteristics in these systems.

Our calculations indicate that the superexchange electronic couplings systematically increase with the increase in the number of fluorine atoms on the acceptor molecules. This can be attributed to the decrease in D–A distances along the stacking directions as a result of an increase in halogen bonding.[14] These results suggest that halogen coupling could have a much stronger effect on the structure–property relations in DA co-crystals than usually expected from a simple picture based on the modification of the molecular electron affinity by

halogenation. The addition of the alkyl side chains (C_n) results in an increase in the distance separating the DA stacks. As a consequence, the direct through-space transfer integrals for both holes and electrons between neighboring stacks is significantly reduced upon substitution of BTBT with a di-C_nBTBT donor.

We have also evaluated the ground-state ionicity parameter of the co-crystals on the basis of the DFT-derived crystal and molecular IR spectra as well as the Mulliken charges. The estimated values of ρ based on Mulliken charges are about 60% smaller than those based on IR vibration mode frequency shifts, with the latter in very good agreement with those based on experimental vibrational data. This indicates that DFT calculations relying on periodic boundary conditions can be used to obtain reliable estimates of ρ in addition to or in the absence of experimental data.

Finally, our calculations indicate that accounting for vibrational-mode mixing (Dushinsky effect) in the frequency-shift based approaches can increase accuracy in the derivation of the ionicity parameters. Consequently, such calculations can provide a better description of the electronic properties of DA co-crystals.

Conflicts of interest

There are no conflicts to declare.

Acknowledgements

References

1 M. Bendikov, F. Wudl and D. F. Perepichka, Tetrathiafulvalenes, oligoacenenes, and their buckminsterfullerene derivatives: The brick and mortar of organic electronics, *Chem. Rev.*, 2004, **104**, 4891.

2 J. E. Anthony, The Larger Acenes: Versatile Organic Semiconductors, *Angew. Chem., Int. Ed.*, 2008, **47**, 452.

3 C. Wang, H. Dong, L. Jiang and W. Hu, Organic semiconductor crystals, *Chem. Soc. Rev.*, 2018, **47**, 422.

4 H. Oberhofer, K. Reuter and J. Blumberger, Charge Transport in Molecular Materials: An Assessment of Computational Methods, *Chem. Rev.*, 2017, **117**, 10319.

5 M. Ball, B. Zhang, Y. Zhong, B. Fowler, S. Xiao, F. Ng, M. Steigerwald and C. Nuckolls, Conjugated Macrocycles in Organic Electronics, *Acc. Chem. Res.*, 2019, **52**, 1068.

6 T. Hasegawa and J. Takeya, Organic field-effect transistors using single crystals, *Sci. Technol. Adv. Mater.*, 2009, **10**, 024314.

7 T. Mori and T. Kawamoto, Organic conductors—from fundamentals to nonlinear conductivity, *Annu. Rep. Prog. Chem., Sect. C: Phys. Chem.*, 2007, **103**, 134.

8 L. Zhu, Y. Yi, Y. Li, E.-G. Kim, V. Coropceanu and J.-L. Brédas, Prediction of Remarkable Ambipolar Charge-Transport Characteristics in Organic Mixed-Stack Charge-Transfer Crystals, *J. Am. Chem. Soc.*, 2012, **134**, 2340.

9 K. P. Goetz, D. Vermeulen, M. E. Payne, C. Kloc, L. E. McNeil and O. D. Jurchescu, Charge-transfer complexes: new perspectives on an old class of compounds, *J. Mater. Chem. C*, 2014, **2**, 3065.

10 L. J. Sun, F. X. Yang, X. T. Zhang and W. P. Hu, Stimuli-responsive behaviors of organic charge transfer cocrystals: recent advances and perspectives, *Mater. Chem. Front.*, 2020, **4**, 715.

11 R. R. Dasari, X. Wang, R. A. Wiscons, H. F. Haneef, A. Ashokan, Y. Zhang, M. S. Fonari, S. Barlow, V. Coropceanu, T. V. Timofeeva, O. D. Jurchescu, J.-L. Brédas, A. J. Matzger and S. R. Marder, Charge-Transport Properties of F6TNAP-Based Charge-Transfer Cocrystals, *Adv. Funct. Mater.*, 2019, **29**, 1904858.

12 R. A. Wiscons, V. Coropceanu and A. J. Matzger, Quaternary Charge-Transfer Solid Solutions: Electronic Tunability through Stoichiometry, *Chem. Mater.*, 2019, **31**, 6598.

13 N. R. Goud, X. P. Zhang, J. L. Bredas, V. Coropceanu and A. J. Matzger, Discovery of Non-linear Optical Materials by Function-Based Screening of Multi-component Solids, *Chem*, 2018, **4**, 150.

14 R. K. Behera, N. R. Goud, A. J. Matzger, J.-L. Brédas and V. Coropceanu, Electronic Properties of 1,5-Diaminonaphthalene:Tetrahalo-1,4-benzoquinone Donor–Acceptor Cocrystals, *J. Phys. Chem. C*, 2017, **121**, 23633.

15 N. Castagnetti, M. Masino, C. Rizzoli, A. Girlando and C. Rovira, Mixed stack charge transfer crystals: Crossing the neutral-ionic borderline by chemical substitution, *Phys. Rev. Mater.*, 2018, **2**, 024602.

16 Y. K. Qin, J. Zhang, X. Y. Zheng, H. Geng, G. Y. Zhao, W. Xu, W. P. Hu, Z. G. Shuai and D. B. Zhu, Charge-Transfer Complex Crystal Based on Extended-Conjugated Acceptor and Sulfur-Bridged Annulene: Charge-Transfer Interaction and Remarkable High Ambipolar Transport Characteristics, *Adv. Mater.*, 2014, **26**, 4093.

17 K. P. Goetz, A. Fonari, D. Vermeulen, P. Hu, H. Jiang, P. J. Diemer, J. W. Ward, M. E. Payne, C. S. Day, C. Kloc, V. Coropceanu, L. E. McNeil and O. D. Jurchescu, Freezing-in orientational disorder induces crossover from thermally-activated to temperature-independent transport in organic semiconductors, *Nat. Commun.*, 2014, **5**, 5642.

18 H. Geng, X. Zheng, Z. Shuai, L. Zhu and Y. Yi, Understanding the Charge Transport and Polarities in Organic Donor–Acceptor Mixed-Stack Crystals: Molecular Insights from the Super-Exchange Couplings, *Adv. Mater.*, 2015, **27**, 1443.

19 J. Zhang, W. Xu, P. Sheng, G. Zhao and D. Zhu, Organic Donor–Acceptor Complexes as Novel Organic Semiconductors, *Acc. Chem. Res.*, 2017, **50**, 1654.

20 H. Geng, L. Y. Zhu, Y. P. Yi, D. B. Zhu and Z. G. Shuai, Superexchange Induced Charge Transport in Organic Donor-Acceptor Cocrystals and Copolymers: A Theoretical Perspective, *Chem. Mater.*, 2019, **31**, 6424.

21 H. Ebata, T. Izawa, E. Miyazaki, K. Takimiya, M. Ikeda, H. Kuwabara and T. Yui, Highly Soluble [1]Benzothieno[3,2-b]benzothiophene (BTBT) Derivatives for High-Performance, Solution-Processed Organic Field-Effect Transistors, *J. Am. Chem. Soc.*, 2007, **129**, 15732.

22 H. Minemawari, T. Yamada, H. Matsui, J. y. Tsutsumi, S. Haas, R. Chiba, R. Kumai and T. Hasegawa, Inkjet printing of single-crystal films, *Nature*, 2011, **475**, 364.

23 K. Nakayama, Y. Hirose, J. Soeda, M. Yoshizumi, T. Uemura, M. Uno, W. Li, M. J. Kang, M. Yamagishi, Y. Okada, E. Miyazaki, Y. Nakazawa, A. Nakao, K. Takimiya and J. Takeya, Patternable Solution-Crystallized Organic Transistors with High Charge Carrier Mobility, *Adv. Mater.*, 2011, **23**, 1626.

24 H. Méndez, G. Heimel, A. Opitz, K. Sauer, P. Barkowski, M. Oehzelt, J. Soeda, T. Okamoto, J. Takeya, J.-B. Arlin, J.-Y. Balandier, Y. Geerts, N. Koch and I. Salzmann, Doping of Organic Semiconductors: Impact of Dopant Strength and Electronic Coupling, *Angew. Chem., Int. Ed.*, 2013, **52**, 7751.

25 J. Tsutsumi, S. Matsuoka, S. Inoue, H. Minemawari, T. Yamada and T. Hasegawa, N-type field-effect transistors based on layered crystalline donor–acceptor semiconductors with dialkylated benzothienobenzothiophenes as electron donors, *J. Mater. Chem. C*, 2015, **3**, 1976.

26 Y. Shibata, J. Tsutsumi, S. Matsuoka, K. Matsubara, Y. Yoshida, M. Chikamatsu and T. Hasegawa, Uniaxially oriented polycrystalline thin films and air-stable n-type transistors based on donor-acceptor semiconductor (diC8BTBT)(FnTCNQ) [n = 0, 2, 4], *Appl. Phys. Lett.*, 2015, **106**, 143303.

27 T. Higashino, M. Dogishi, T. Kadoya, R. Sato, T. Kawamoto and T. Mori, Air-stable n-channel organic field-effect transistors based on charge-transfer complexes including dimethoxybenzothienobenzothiophene and tetracyanoquinodimethane derivatives, *J. Mater. Chem. C*, 2016, **4**, 5981.

28 R. Sato, M. Dogishi, T. Higashino, T. Kadoya, T. Kawamoto and T. Mori, Charge-Transfer Complexes of Benzothienobenzothiophene with Tetracyanoquinodimethane and the n-Channel Organic Field-Effect Transistors, *J. Phys. Chem. C*, 2017, **121**, 6561.

29 N. Castagnetti, A. Girlando, M. Masino, C. Rizzoli and C. Rovira, Mixed Stack Organic Semiconductors: The Anomalous Case of the BTBT-TCNQFx Series, *Cryst. Growth Des.*, 2017, **17**, 6255.

30 Z. P. Zhang, L. Jiang, C. L. Cheng, Y. G. Zhen, G. Y. Zhao, H. Geng, Y. P. Yi, L. Q. Li, H. L. Dong, Z. G. Shuai and W. P. Hu, The Impact of Interlayer Electronic Coupling on Charge Transport in Organic Semiconductors: A Case Study on Titanylphthalocyanine Single Crystals, *Angew. Chem., Int. Ed.*, 2016, **55**, 5206.

31 R. Sato, T. Kawamoto and T. Mori, Asymmetrical hole/electron transport in donor-acceptor mixed-stack cocrystals, *J. Mater. Chem. C*, 2019, **7**, 567.

32 R. L. Martin, Natural transition orbitals, *J. Chem. Phys.*, 2003, **118**, 4775.

33 M. J. Frisch, G. W. Trucks, H. B. Schlegel, G. E. Scuseria, M. A. Robb, J. R. Cheeseman, G. Scalmani, V. Barone, B. Mennucci, G. A. Petersson, H. Nakatsuji, M. Caricato, X. Li, H. P. Hratchian, A. F. Izmaylov, J. Bloino, G. Zheng, J. L. Sonnenberg, M. Hada, M. Ehara, K. Toyota, R. Fukuda, J. Hasegawa, M. Ishida, T. Nakajima, Y. Honda, O. Kitao, H. Nakai, T. Vreven, J. A. Montgomery Jr., J. E. Peralta, F. Ogliaro, M. J. Bearpark, J. Heyd, E. N. Brothers, K. N. Kudin, V. N. Staroverov, R. Kobayashi, J. Normand, K. Raghavachari, A. P. Rendell, J. C. Burant, S. S. Iyengar, J. Tomasi, M. Cossi, N. Rega, N. J. Millam, M. Klene, J. E. Knox, J. B. Cross, V. Bakken, C. Adamo, J. Jaramillo, R. Gomperts, R. E. Stratmann, O. Yazyev, A. J. Austin, R. Cammi, C. Pomelli, J. W. Ochterski, R. L. Martin, K. Morokuma, V. G. Zakrzewski, G. A. Voth, P. Salvador, J. J. Dannenberg, S. Dapprich, A. D. Daniels, Ö. Farkas, J. B. Foresman, J. V. Ortiz, J. Cioslowski and D. J. Fox, *Gaussian 09, Revision D. 01*, Gaussian, Inc., Wallingford, CT, 2009.

34 M. Rérat, L. Maschio, B. Kirtman, B. Civalleri and R. Dovesi, Computation of Second Harmonic Generation for Crystalline Urea and KDP. An ab Initio Approach through the Coupled Perturbed Hartree–Fock/Kohn–Sham Scheme, *J. Chem. Theory Comput.*, 2016, **12**, 107.

35 R. Dovesi, A. Erba, R. Orlando, C. M. Zicovich-Wilson, B. Civalleri, L. Maschio, M. Rérat, S. Casassa, J. Baima, S. Salustro and B. Kirtman, Quantum-mechanical condensed matter simulations with CRYSTAL, *Wiley Interdiscip. Rev.: Comput. Mol. Sci.*, 2018, **8**, e1360.

36 R. Dovesi, R. Orlando, A. Erba, C. M. Zicovich-Wilson, B. Civalleri, S. Casassa, L. Maschio, M. Ferrabone, M. De La Pierre, P. D'Arco, Y. Noël, M. Causà, M. Rérat and B. Kirtman, CRYSTAL14: A program for the ab initio investigation of crystalline solids, *Int. J. Quantum Chem.*, 2014, **114**, 1287.

37 L. Zhu, Y. Yi, A. Fonari, N. S. Corbin, V. Coropceanu and J.-L. Brédas, Electronic Properties of Mixed-Stack Organic Charge-Transfer Crystals, *J. Phys. Chem. C*, 2014, **118**, 14150.

38 V. Coropceanu, J. Cornil, D. A. da Silva Filho, Y. Olivier, R. Silbey and J.-L. Brédas, Charge Transport in Organic Semiconductors, *Chem. Rev.*, 2007, **107**, 926.

39 K. Seeger, *Semiconductor physics: an introduction*, Berlin: Springer, Berlin, 9th edn, 2010.

40 L. Zhu, H. Geng, Y. Yi and Z. Wei, Charge transport in organic donor–acceptor mixed-stack crystals: the role of nonlocal electron–phonon couplings, *Phys. Chem. Chem. Phys.*, 2017, **19**, 4418.

41 R. S. Mulliken, Molecular Compounds and their Spectra. II, *J. Am. Chem. Soc.*, 1952, **74**, 811.

42 N. S. Hush, Homogeneous and heterogeneous optical and thermal electron transfer, *Electrochim. Acta*, 1968, **13**, 1005.

43 V. Coropceanu, X.-K. Chen, T. Wang, Z. Zheng and J.-L. Brédas, Charge-transfer electronic states in organic solar cells, *Nat. Rev. Mater.*, 2019, **4**, 689.

44 E. Kampar and O. Neilands, Degree of Charge Transfer in Donor–Acceptor Systems of the π–π Type, *Russ. Chem. Rev.*, 1986, **55**, 334.

45 D. Vermeulen, L. Y. Zhu, K. P. Goetz, P. Hu, H. Jiang, C. S. Day, O. D. Jurchescu, V. Coropceanu, C. Kloc and L. E. McNeil, Charge Transport Properties of Perylene–TCNQ Crystals: The Effect of Stoichiometry, *J. Phys. Chem. C*, 2014, **118**, 24688.

46 J. R. Reimers, A practical method for the use of curvilinear coordinates in calculations of normal-mode-projected

3630 | *Mater. Chem. Front.*, 2020, **4**, 3623–3631

This journal is © The Royal Society of Chemistry and the Chinese Chemical Society 2020

displacements and Duschinsky rotation matrices for large molecules, *J. Chem. Phys.*, 2001, **115**, 9103.

47 A. Fonari, C. Sutton, J.-L. Brédas and V. Coropceanu, Impact of exact exchange in the description of the electronic structure of organic charge-transfer molecular crystals, *Phys. Rev. B: Condens. Matter Mater. Phys.*, 2014, **90**, 165205.

48 L. Kronik and S. Kümmel, Dielectric Screening Meets Optimally Tuned Density Functionals, *Adv. Mater.*, 2018, **30**, 1706560.

49 Z. Zheng, D. A. Egger, J.-L. Brédas, L. Kronik and V. Coropceanu, Effect of Solid-State Polarization on Charge-Transfer Excitations and Transport Levels at Organic Interfaces from a Screened Range-Separated Hybrid Functional, *J. Phys. Chem. Lett.*, 2017, **8**, 3277.